Research Article Vol. 30, No. 15 / 18 Jul 2022 / Optics Express 27983
Optics EXPRESS

High wall-plug efficiency and narrow linewidth III-V-on-silicon C-band DFB laser diodes

JAVAD RAHIMI VASKASI,[1,2,*] NISHANT SINGH,[3] JORIS VAN KERREBROUCK,[3] JOHAN BAUWELINCK,[3] GUNTHER ROELKENS,[1,2] AND GEERT MORTHIER[1,2]

[1] *Photonics Research Group, Ghent University-IMEC, 9052 Ghent, Belgium*
[2] *Center for Nano-and Biophotonics (NB-Photonics), Ghent University, Ghent B- 9000, Belgium*
[3] *IDLab, Ghent University-IMEC, 9052 Ghent, Belgium*
[*] *javad.rahimi@ugent.be*

Abstract: We present recent results on compact and power efficient C-band distributed feedback lasers through adhesive bonding of a III-V die onto a silicon-on-insulator circuit. A wall-plug efficiency up to 16% is achieved for bias currents below 40 mA. The laser cavity is 180 μm long and a single facet output power up to 11 mW is measured at 20 °C by incorporating a broadband reflector in the silicon waveguide at one side of the cavity. Single mode operation at 1567 nm with a side mode suppression ratio of around 55 dB is demonstrated. By controlling the phase of the external feedback, the laser linewidth is decreased to 28 kHz. Measurement result shows a low relative intensity noise below -150 dB/Hz at 60 mA up to 6 GHz. We also report 20 and 10 Gbps data transmission at a bias current of 50 mA at 20 °C and 40 °C, respectively.

1. Introduction

Integration of photonics and electronics is a prerequisite for the future datacom transceivers to limit the power consumption for interconnects at speeds of tens of Gbps. Silicon photonics is then often preferred as it allows integrating optical transceivers on a silicon-on-insulator (SOI) platform [1,2]. During the past decade, there have been rapid advances both in research and commercialization of silicon photonics components. High-performance passive components such as optical waveguides and couplers can be realized on SOI using mature CMOS fabrication processes [3]. Additionally, high-performance silicon optical modulators based on the plasma dispersion effect have been demonstrated successfully [1]. Germanium, which is a CMOS compatible material enables the fabrication of ultra-fast photodiodes on silicon [4]. However, due to their indirect bandgap structure, it is impossible to realize efficient light sources in silicon or germanium. This issue leads to the need for integrating III-V materials onto SOI to realize efficient light sources at 1.3 or 1.55 μm.

Different integration methods have been used to combine III-V lasers with silicon photonics. The hybrid integration has been demonstrated as a viable approach in providing the required optical sources [5,6]. However, challenges such as scaling limitations and alignment precision limit the applications of this approach. Another promising approach is the direct epitaxial growth of III-V materials on the Si substrate. While high performance light sources based on quantum dot active regions have been fabricated using this technique [7,8], due to the high density of the threading dislocations (TDs) caused by the mismatch of lattice constants and thermal expansion coefficients, it is difficult to achieve high quality layers for efficient lasing in multiple quantum well (MQW) lasers [9]. Heterogeneous integration proved to be another viable alternative for the realization of high-performance compact lasers onto SOI platform. This technique is mainly based on bonding or micro-transfer printing. In molecular or adhesive bonding, the III-V material is first bonded to Si and then processed into active components such as lasers or amplifiers. In the micro-transfer printing technique, the III-V material is first processed on its own substrate to

#462051 https://doi.org/10.1364/OE.462051
Journal © 2022 Received 22 Apr 2022; revised 24 Jun 2022; accepted 5 Jul 2022; published 15 Jul 2022

Optics EXPRESS

make components as coupons, and then these coupons can be transferred to an SOI photonic integrated circuit to fabricate lasers or in general photonic integrated circuits [10–12].

There has been a lot of progress in the demonstration of heterogeneously integrated lasers during the past decade. While vertical cavity surface emitting lasers (VCSELs) can be good candidates for interconnects due to their compactness and low threshold, their limited optical power makes them less desirable for integrated wavelength-division multiplexing (WDM) modules [9]. On the other hand, edge emitting laser diodes such as distributed feedback (DFB) or distributed Bragg reflector (DBR) lasers are suitable for the fabrication of compact WDM sources, but have suffered from somewhat lower wall-plug efficiency in the past. A high wall-plug efficiency normally leads to a low electrical power consumption for the optical transmitter and requires typically also less power consuming cooling. This is especially important where many transmitters are present in a limited area (e.g., in datacenters). Additionally, low noise semiconductor lasers with high output power are required in many applications such as coherent communications systems and LIDAR remote sensing [13]. Low noise performance is characterised by low frequency-noise (or linewidth) and low relative-intensity noise (RIN). Regarding the coherent communications, the detection of the encoded signal on the phase of the laser light can be disturbed and an error will be detected if there are severe instabilities in the phase of the laser light. These instabilities known as phase noise can be described as an intrinsic linewidth of the laser. In a LIDAR system, a narrow linewidth increases the coherence length of the laser light which results in boosting the detection range of the LIDAR system and makes the system less vulnerable to the speckle effect [14]. Heterogeneous integration enables realization of low linewidth lasers in low loss silicon or silicon nitride platforms [13,15,16]. In this regard, novel designs with better efficiency, lower intrinsic linewidth and RIN as well as high-speed direct modulation potential are being investigated.

In [17], high performance long cavity III-V-on-Si DFB lasers with a threshold current of around 35 mA at 20 °C and a wall-plug efficiency of about 9% at a bias current of 90 mA were reported. The measured laser linewidth and the side mode suppression ratio (SMSR) were around 1MHz and 50 dB, respectively. [18] demonstrated low threshold short-cavity integrated DFB lasers with wall plug efficiencies up to 3% at 1mW output power. A SMSR larger than 55 dB as well as a 12.5 Gbps direct modulation were achieved. Intel reported high performance heterogeneously integrated DFB lasers operating in the O-band with a wall plug efficiency of 15% at 80 °C [19]. However, neither direct modulation nor linewidth characterization results have been reported. At the expense of more complex fabrication by using a combination of direct bonding and epitaxial regrowth, short cavity membrane lasers on the SiO_2/Si substrate have been demonstrated [20,21]. A brief review on static and dynamic behavior of demonstrated heterogeneously integrated DFB lasers is provided in [22]. The low noise performance of heterogeneously integrated semiconductor lasers also has been investigated thoroughly. In order to decrease the fundamental linewidth of semiconductor lasers, the quantum phase noise has to be reduced by controlling the spontaneous emission in the cavity. Regarding the III-V-on-Si DFB lasers, pushing down the fundamental optical mode into the silicon underneath can result in a lower optical loss as well as less overlap with the active region. This concept has been applied in [23,24] by adding a 150 nm planarized oxide spacer to increase the optical mode confinement in the silicon waveguide. The low quantum well confinement of about 0.2% resulted in a measured sub-kHz linewidth as well as a high robustness to optical feedback [25,26]. However, a very high threshold current due to the low confinement factor in the active region and a high grating reflection limit the maximum output power (to a few mW) of these mm length devices. Other efforts in demonstrating low linewidth integrated lasers have focused on extended (external) cavity lasers. Heterogeneous integration enables the optimization of active and passive sections of external cavity lasers independently and more efficiently. [16,27,28].

Optics EXPRESS

In this paper, we present heterogeneously integrated compact DFB lasers with high efficiency, low noise, and high modulation bandwidth. First, we describe the design and fabrication of the devices. Then the static characterization of a fabricated laser including the frequency and intensity noise characteristics is discussed. In order to investigate the dynamic response of the laser, a set of small signal and large signal data transmission experiments have been done. We end with proposals for further improvements.

2. Laser structure and fabrication

Fig. 1 depicts the schematic of the reported devices. A 400 nm thick Si device layer on top of a 2 µm buried oxide layer is used. The cavity, determined by a first order, quarter-wave-shifted grating is 180 µm long. The DFB grating is patterned into the SOI using a Voyager electron beam lithography (EBL) system. Figure 2(a) shows the dependence of the fundamental optical mode confinement factor in the MQW active region on the width of the III-V mesa and the silicon waveguide. Decreasing the width of the III-V mesa can be useful in pushing the mode down into the silicon leading to a lower internal loss. However, it can also be detrimental for the device series resistance, specifically for short cavity lasers, as well as for the provision of sufficient gain for lasing. While a wider silicon waveguide can be also advantageous in pushing down the optical mode into the silicon waveguide and decreasing the internal loss of the cavity, it can result in excitation of higher order modes and affect the laser performance.

Designing a narrow III-V mesa and Si waveguide together with a narrower DFB grating in the middle of the silicon waveguide can be beneficial in suppressing the excitation of the higher order mode which extends towards the edges of the waveguide. The width of the grating is chosen to be 1 µm and that of the III-V mesa and the silicon waveguide is chosen to be 2 µm. The 6 µm wide active region consists of six QW layers each 6 nm thick, separated by 10 nm barriers in between. Figures 2(b-d) illustrate the effect of the DFB grating etch depth on the confinement factor in MQW active region, the internal loss of the cavity , and the grating coupling coefficient (κ). In this design the DFB grating and the silicon waveguide are defined with a 40 nm etch. This shallow etch configuration allows the optical mode to be predominantly confined to the silicon, which not only facilitates the light coupling from the III-V to the silicon waveguide underneath but is also beneficial in decreasing the internal loss since the III-V cladding layers are highly absorbing. A 14 µm long linear taper is sufficient to get over 90% of coupling. Then the shallow etched part of the structure is connected to a 180 nm etched, 2 µm wide silicon rib waveguide. In order to increase the single facet output power, a broadband reflector is incorporated in the silicon waveguide at one side of the cavity. In Fig. 1, the optical mode profiles in the middle of the cavity and at the taper tip are shown. As reported in figure 2(b) the simulated confinement factor in the MQW active region, consisting of InGaAsP MQW layers, is 3.5%. These devices are realized using adhesive bonding in which the III-V epitaxial layer is bonded onto the pre-patterned SOI. The full description of the fabrication steps can be found in [22].

Optics EXPRESS

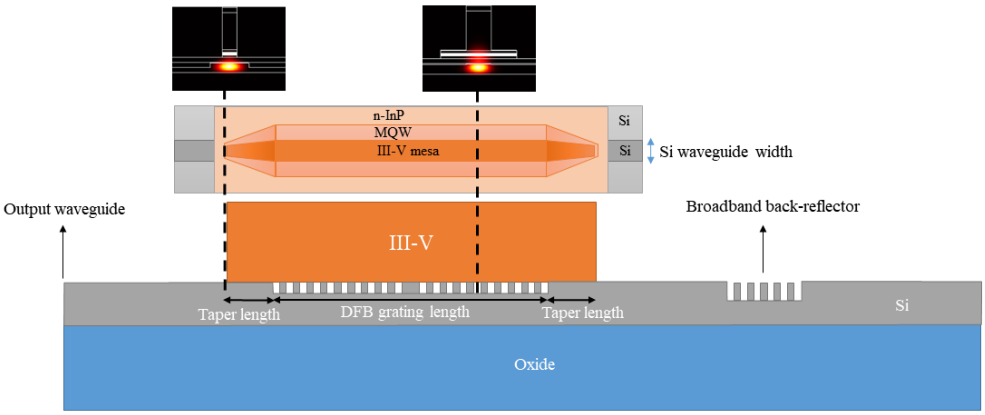

Fig. 1. The schematic of a fabricated heterogeneously integrated III-V-on-Si C-band DFB laser.

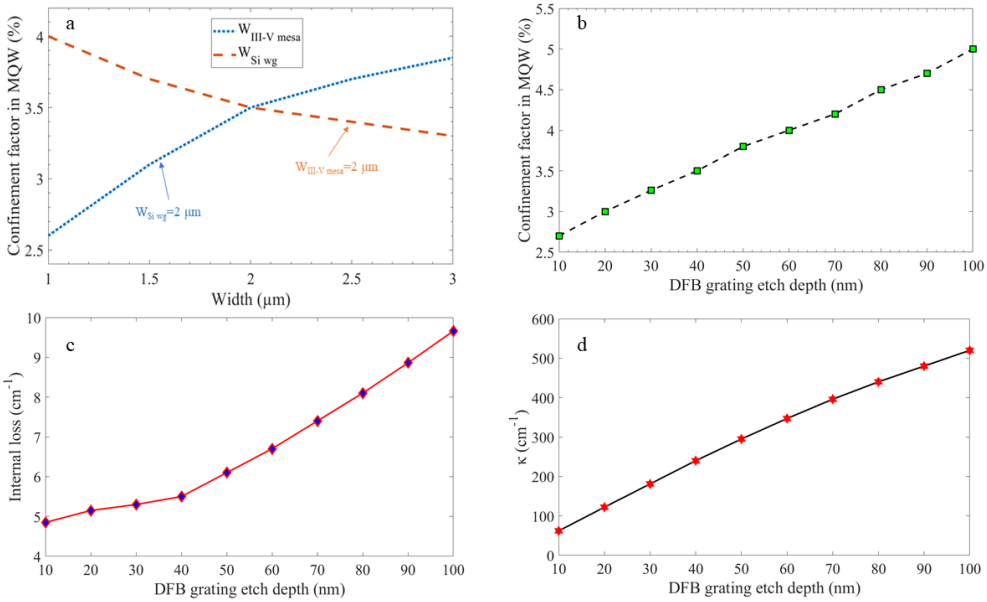

Fig. 2. Simulation results for the confinement factor in MQW, the internal loss , and the grating coupling coefficient. a) Confinement factor in the MQW active region versus the width of the III-V meas and the silicon waveguide, b) Confinement factor in the MQW active region versus the DFB grating etch depth, c) Internal loss versus the DFB grating etch depth, and d) DFB grating coupling coefficient κ versus the DFB grating etch depth.

Optics EXPRESS

3. Experimental results

3.1. Static characterization

Fig. 3 shows the static characteristics of the fabricated device. The laser is mounted on a stage equipped with a temperature controller and is biased with a Keithley 2400 source meter. The output light is collected through a fiber-to-chip grating coupler with a 9 dB measured coupling loss. In Fig. 3(a) the single facet output optical power is plotted for two different lasers. In our previous work in [22] the DFB laser has a symmetric configuration with equal output power from both facets. However, in this work due to an HR facet at one side of the cavity the laser just has one output facet. As can be seen, at 20 °C the laser has a threshold current of 11 mA and an output power of up to 11 mW is coupled to the silicon waveguide. By increasing the stage temperature to 40 °C, the threshold current increases to 15 mA. The measured series resistance is about 9 Ω for the 180 µm long cavity. As can be derived from Fig. 3(b), the lasing wavelength is 1567 nm and the SMSR is around 55 dB at 60 mA.

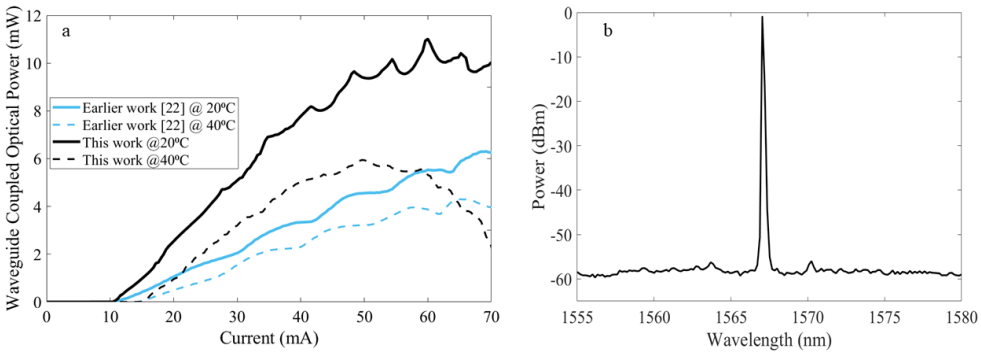

Fig. 3. Static characteristics of the current device and an earlier device. a) waveguide-coupled optical output power, b) the optical spectrum at a bias current of 60 mA at 20 °C.

The DFB grating coupling coefficient κ can be extracted from the full stopband visible in the laser spectrum shown in Fig 3(b), using the following equation [29]:

$$\Delta\lambda = \frac{\lambda_B^2}{2\pi n_{eff} L_o}\sqrt{(\kappa L_o)^2 + 4\pi^2} \tag{1}$$

where $\Delta\lambda$ is the half width of the full stopband, λ_B denotes the Bragg wavelength, n_{eff} represents the effective index of the lasing mode, and L_o is the effective or optical length of the cavity. Since there is an HR facet at one side of the DFB cavity the L_o is equal to 2L where L is the DFB grating length (cavity length) equal to 180 µm in this work. By inserting $\Delta\lambda$= 3.5 nm from the spectrum, the κ value of 233 cm^{-1} is obtained, which is in good agreement with the simulated value of around 240 cm^{-1} reported in Fig. 2(d). We choose an etch depth of 40 nm as this combines small internal loss and high κL.

In order to investigate more the performance of the device in terms of wall-plug efficiency, an intuitive analysis based on experimental results is useful. In Fig 3(a), by considering the slope efficiency at 20 mA at 20 °C, the ratio of the internal loss α_{int} to the mirror loss α_m is found to be 2.2, assuming a 100 % injection efficiency. The simulated internal loss for a DFB grating etch depth of 40 nm is around 5.4 cm^{-1} (Fig 2(c)) from which a mirror loss of 2.45 cm^{-1} can be estimated for this cavity. According to [29], a mirror loss range of 0.21 $cm^{-1} < \alpha_m < 7.7\ cm^{-1}$ can be found for the structure represented in this study. The mirror loss strongly depends on the equivalent phase shift. From the optical spectrum of Fig. 3(b), the phase shift is close to, but not

Optics EXPRESS

equal to $\lambda/4$. To increase the wall-plug efficiency of the lasers reported in this work, the ratio of α_{int}/α_m needs to be unity or close to unity which means the κL value has to be reduced. This can be achieved by decreasing the etch depth of the DFB grating or using a narrower DFB grating.

Fig. 4 gives the wall-plug efficiency versus the injected current for two cases. In our previous work, the wall-plug efficiency is plotted by adding the output power from both facets. In this work, more than 16% wall-plug efficiency is achieved at 20 °C for bias currents below 40 mA which shows an improvement of 4 % compared to our previous work. It also shows the laser performance in a semi-cooled operation regime with a wall-plug efficiency up to 10%.

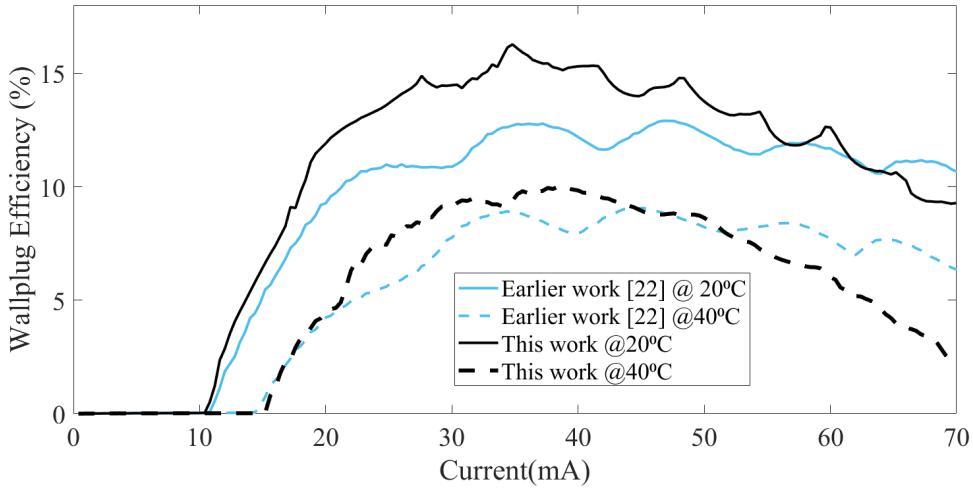

Fig. 4. Illustration of the measured wall-plug efficiency versus the injected current.

We then measured the spectral densities of the frequency and relative intensity noise of the laser. The spectrum of the frequency noise of the laser was measured using a OE4000 phase and frequency noise test system without using an optical isolator, while the RIN was measured with an electrical spectrum analyzer. Fig. 5 depicts the frequency noise spectra at the bias current of 60 mA. The power spectral density (PSD) of the Gaussian white noise is found to be 140×10^3 Hz^2/Hz at 20 °C. An intrinsic (Lorentzian) linewidth of 440 kHz has been calculated by multiplying the white noise PSD value by π. Besides the low loss silicon platform, this reduction in the solitary laser linewidth can also be attributed to the weak feedback effect of the external cavity formed by the grating coupler. In our design, the output grating coupler is placed at the distance of 1350 μm from the nearest laser facet and the broadband reflector is approximately 90 μm away from the other facet which constitutes a compound cavity with the total length of 1620 μm. The variation of the linewidth with the phase of the external reflection has been described in [30]. We changed this phase by changing the temperature of the stage and the measured intrinsic linewidth versus the temperature is shown in the inset shown in Fig. 5. This causes sufficient changes in lasing wavelength to change the phase of the reflection over 2π. We found that tuning the operating temperature can lead to a significant decrease in the laser linewidth. The measured frequency noise spectrum at 22 °C plotted in Fig. 5 shows a white noise PSD of 8870 Hz^2/Hz which corresponds to a intrinsic linewidth of 28 kHz.

The RIN is measured at 20 °C by connecting the fiber coupled optical output of the laser to a high speed DSC-R409 Lab Buddy optical receiver. Then the output electrical signal from the receiver is sent to a low noise SHF S804B amplifier to overcome the limited noise floor of the spectrum analyzer at the end of the link. The noise measurement is performed up to 20 GHz, once after switching the laser off to measure the total thermal noise of the link and then after

Optics EXPRESS

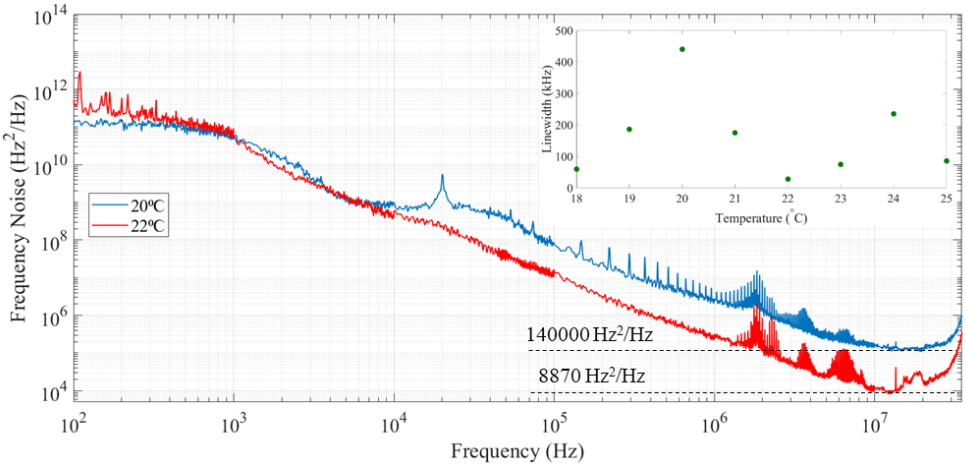

Fig. 5. The spectral density of the frequency noise versus frequency of the heterogeneously integrated DFB laser. The Lorenzian linewidth is calculated by multiplying the white noise level (the flat part of the spectra) by π. The measured intrinsic linewidth versus the temperature is shown in the inset.

turning it on to measure the total noise including the contribution from the intensity noise of the laser. The laser RIN is then calculated by subtracting the thermal noise from the total measured noise. The shot noise of the receiver is found to be around -177 dB/Hz which is not a limiting factor in this measurement. In Fig. 6, the measured RIN at bias currents of 50 mA and 60 mA are depicted. The laser RIN is below -150 dB/Hz up to 6 GHz.

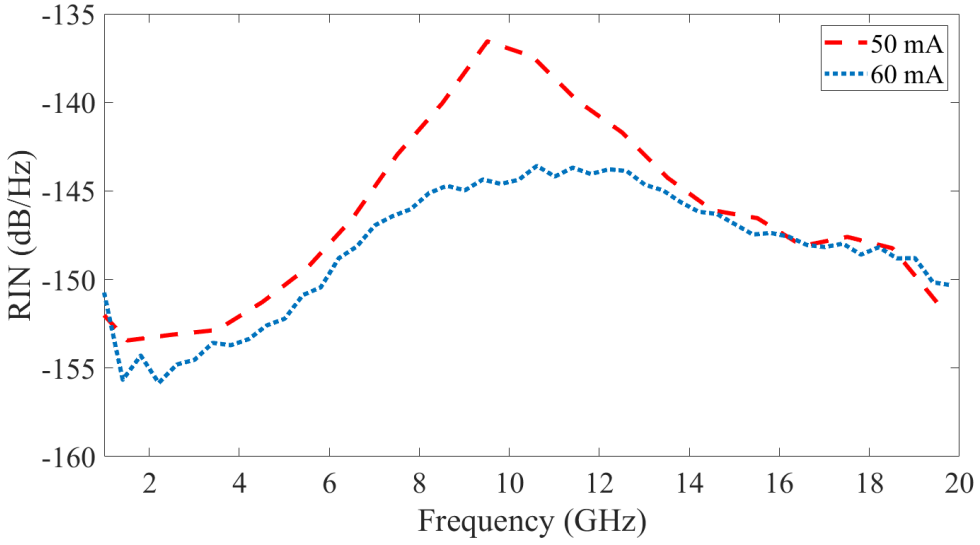

Fig. 6. RIN measured from the reported III-V-on-Si DFB laser at bias currents of 50 mA and 60 mA at 20 °C.

Optics EXPRESS

3.2. Dynamic characterization

In order to investigate the dynamic behavior of the device, a set of small signal modulation and large signal data transmission experiments have been carried out. Regarding the small signal modulation experiment, the laser is biased using an Agilent N5247A vector network analyzer (VNA) to provide radio frequency (RF) electrical signals. The optical signal of the laser is captured by a Discovery DSC-10H photodetector (PD) and the corresponding output electrical signal is connected to the VNA to measure the small signal S parameters. Fig. 7(a) shows the small signal behavior of the laser at 20 °C and 40 °C with a modulation bandwidth of about 14 GHz and 9 GHz at 50 mA, respectively. The data transmission experiment is performed by using a Keysight M8196A arbitrary waveform generator (AWG). The modulated output of the laser is directly connected to a high-speed PD without using any optical or electrical amplifier nor equalization. Fig. 7(b) and (c) show the eye diagrams for NRZ data transmission with a Pseudo-Random-Binary-Sequence (PRBS) pattern length of 2^9-1 at 20 Gbps and 10 Gbps at 20 °C and 40 °C, respectively.

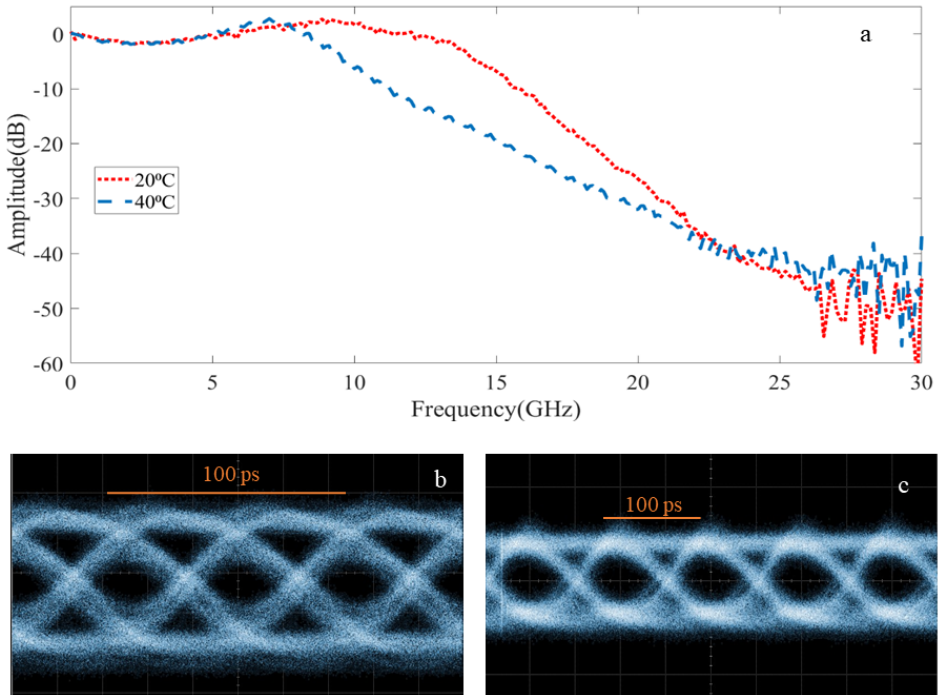

Fig. 7. Dynamic characterization of the device. a) small signal response at 20 °C and 40 °C, b) eye diagram for the 20 Gbps back to back data transmission at 20 °C, and c) eye diagram for the 10 Gbps back to back data transmission at 40 °C.

4. Conclusion

In this paper, we demonstrated a compact and high-efficiency integrated DFB laser realized by the adhesive bonding technique. By using a shallow etched grating in the DFB cavity, the optical mode is predominantly confined to the silicon underneath. This is beneficial in decreasing the laser threshold current and increasing the slope efficiency as well as in reducing the Lorentzian linewidth by decreasing the internal loss in the cavity. In order to increase the single facet output power, a deeply etched broadband reflector is incorporated in the silicon waveguide at one side of the cavity. Our measurement results show wall-plug efficiencies up to 16% and 10% at

Optics EXPRESS

temperatures of 20 °C and 40 °C, respectively. For further investigation of the device performance, the frequency and intensity noise of the laser have been measured. A very low frequency noise is obtained by taking advantage of a low loss short external cavity formed by the weak feedback from the grating coupler. It is shown that by a 2 °C increase in the temperature the Lorentzian linewidth can be decreased more than an order of magnitude to a value as low as 28 kHz. In addition, the RIN is measured below -150 dB/Hz up to 6 GHz. Dynamic characterization of the laser has also been carried out and 20 and 10 Gbps directly modulated data transmission have been reported at a bias current of 50 mA at 20 °C and 40 °C, respectively. Further improvement could still be expected by optimizing the etching of the InP mesa to reduce scattering loss or by decreasing the mirror loss by reducing the DFB grating coupling coefficient κ. Using a narrower active layer would improve the confinement factor over volume ratio and thus also the modulation bandwidth. The narrower active layer will most likely also reduce the leakage current and thus result in lower threshold current and still higher efficiency.

Funding. Methusalem program of the Flemish government.

Acknowledgments. J. Rahimi would like to thank M. Muneeb for support in preparation of the SOI circuit using EBL and L. Van Landschoot for FIB images.

Disclosures. The authors declare no conflicts of interest.

Data availability. Data underlying the results presented in this paper are not publicly available at this time but may be obtained from the authors upon reasonable request.

References

1. H. Mekawey, M. Elsayed, Y. Ismail, and M. A. Swillam, "Optical interconnects finally seeing the light in silicon photonics: Past the hype," Nanomaterials **12**(3), 485 (2022).
2. N. Margalit, C. Xiang, S. M. Bowers, A. Bjorlin, R. Blum, and J. E. Bowers, "Perspective on the future of silicon photonics and electronics," Appl. Phys. Lett. **118**(22), 220501 (2021).
3. C. A. Thraskias, E. N. Lallas, N. Neumann, L. Schares, B. J. Offrein, R. Henker, D. Plettemeier, F. Ellinger, J. Leuthold, and I. Tomkos, "Survey of photonic and plasmonic interconnect technologies for intra-datacenter and high-performance computing communications," IEEE Commun. Surv. Tutor. **20**(4), 2758–2783 (2018).
4. S. Lischke, A. Peczek, J. Morgan, K. Sun, D. Steckler, Y. Yamamoto, F. Korndörfer, C. Mai, S. Marschmeyer, M. Fraschke, A. Krüger, A. Beling, and L. Zimmermann, "Ultra-fast germanium photodiode with 3-db bandwidth of 265 ghz," Nat. Photonics **15**(12), 925–931 (2021).
5. M. Billah, T. Hoose, T. Onanuga, N. Lindenmann, P. Dietrich, T. Wingert, M. Goedecke, A. Hofmann, U. Troppenz, M. Moehrle, A. Sigmund, W. Freude, and C. Koos, "Multi-chip integration of lasers and silicon photonics by photonic wire bonding," in *2015 Conference on Lasers and Electro-Optics (CLEO)*, (IEEE, 2015), pp. 1–2.
6. C. Gunn, "Cmos photonics for high-speed interconnects," IEEE Micro **26**(2), 58–66 (2006).
7. A. Y. Liu, C. Zhang, J. Norman, A. Snyder, D. Lubyshev, J. M. Fastenau, A. W. Liu, A. C. Gossard, and J. E. Bowers, "High performance continuous wave 1.3 μ m quantum dot lasers on silicon," Appl. Phys. Lett. **104**(4), 041104 (2014).
8. S. Chen, W. Li, J. Wu, Q. Jiang, M. Tang, S. Shutts, S. N. Elliott, A. Sobiesierski, A. J. Seeds, I. Ross, P. M. Smowton, and H. Liu, "Electrically pumped continuous-wave iii–v quantum dot lasers on silicon," Nat. Photonics **10**(5), 307–311 (2016).
9. S. Matsuo and T. Kakitsuka, "Low-operating-energy directly modulated lasers for short-distance optical interconnects," Adv. Opt. Photonics **10**(3), 567–643 (2018).
10. A. W. Fang, H. Park, O. Cohen, R. Jones, M. J. Paniccia, and J. E. Bowers, "Electrically pumped hybrid algainas-silicon evanescent laser," Opt. Express **14**(20), 9203–9210 (2006).
11. J. Zhang, G. Muliuk, J. Juvert, S. Kumari, J. Goyvaerts, B. Haq, C. Op de Beeck, B. Kuyken, G. Morthier, D. Van Thourhout, R. Baets, G. Lepage, P. Verheyen, J. Van Campenhout, A. Gocalinska, J. O'Callaghan, E. Pelucchi, T. Kevin, B. Corbett, A. J. Trindade, and G. Roelkens, "Iii-v-on-si photonic integrated circuits realized using micro-transfer-printing," APL Photonics **4**(11), 110803 (2019).
12. B. Haq, J. R. Vaskasi, J. Zhang, A. Gocalinska, E. Pelucchi, B. Corbett, and G. Roelkens, "Micro-transfer-printed iii-v-on-silicon c-band distributed feedback lasers," Opt. Express **28**(22), 32793–32801 (2020).
13. D. Huang, M. A. Tran, J. Guo, J. Peters, T. Komljenovic, A. Malik, P. A. Morton, and J. E. Bowers, "High-power sub-khz linewidth lasers fully integrated on silicon," Optica **6**(6), 745–752 (2019).
14. P. F. McManamon, *LIDAR Technologies and Systems*, vol. PM300 (SPIE, 2019).
15. C. T. Santis, S. T. Steger, Y. Vilenchik, A. Vasilyev, and A. Yariv, "High-coherence semiconductor lasers based on integral high-q resonators in hybrid si/iii-v platforms," Proc. Natl. Acad. Sci. U. S. A. **111**(8), 2879–2884 (2014).
16. C. Xiang, J. Guo, W. Jin, L. Wu, J. Peters, W. Xie, L. Chang, B. Shen, H. Wang, Q.-F. Yang, L. Wu, D. Kinghorn, M. Paniccia, K. J. Vahala, P. A. Morton, and J. E. Bowers, "High-performance lasers for fully integrated silicon nitride photonics," Nat. Commun. **12**(1), 1–8 (2021).

Optics EXPRESS

17. S. Keyvaninia, S. Verstuyft, L. Van Landschoot, F. Lelarge, G.-H. Duan, S. Messaoudene, J. Fedeli, T. De Vries, B. Smalbrugge, E. Geluk, J. Bolk, M. Smit, G. Morthier, D. Van Thourhout, and G. Roelkens, "Heterogeneously integrated iii-v/silicon distributed feedback lasers," Opt. Lett. **38**(24), 5434–5437 (2013).
18. C. Zhang, S. Srinivasan, Y. Tang, M. J. Heck, M. L. Davenport, and J. E. Bowers, "Low threshold and high speed short cavity distributed feedback hybrid silicon lasers," Opt. Express **22**(9), 10202–10209 (2014).
19. R. Jones, P. Doussiere, J. B. Driscoll, W. Lin, H. Yu, Y. Akulova, T. Komljenovic, and J. E. Bowers, "Heterogeneously integrated inp\/silicon photonics: fabricating fully functional transceivers," IEEE Nanotechnol. Mag. **13**(2), 17–26 (2019).
20. S. Matsuo, T. Fujii, K. Hasebe, K. Takeda, T. Sato, and T. Kakitsuka, "Directly modulated buried heterostructure dfb laser on sio 2/si substrate fabricated by regrowth of inp using bonded active layer," Opt. Express **22**(10), 12139–12147 (2014).
21. S. Yamaoka, N.-P. Diamantopoulos, H. Nishi, R. Nakao, T. Fujii, K. Takeda, T. Hiraki, T. Tsurugaya, S. Kanazawa, H. Tanobe, T. Kakitsuka, T. Tsuchizawa, F. Koyama, and S. Matsuo, "Directly modulated membrane lasers with 108 ghz bandwidth on a high-thermal-conductivity silicon carbide substrate," Nat. Photonics **15**(1), 28–35 (2021).
22. J. Rahimi, J. Van Kerrebrouck, B. Haq, J. Bauwelinck, G. Roelkens, and G. Morthier, "Demonstration of a high-efficiency short-cavity iii-v-on-si c-band dfb laser diode," IEEE J. Sel. Top. Quantum Electron. **28**(3), 1–6 (2022).
23. C. T. Santis, Y. Vilenchik, N. Satyan, G. Rakuljic, and A. Yariv, "Quantum control of phase fluctuations in semiconductor lasers," Proc. Natl. Acad. Sci. U. S. A. **115**(34), E7896–E7904 (2018).
24. C. T. Santis, Y. Vilenchik, A. Yariv, N. Satyan, and G. Rakuljic, "Sub-khz quantum linewidth semiconductor laser on silicon chip," in *CLEO: Applications and Technology*, (Optical Society of America, 2015), pp. JTh5A–7.
25. Z. Zhang, H. Wang, N. Satyan, G. Rakuljic, C. T. Santis, and A. Yariv, "Coherent and incoherent optical feedback sensitivity of high-coherence si/iii-v hybrid lasers," in *Optical Fiber Communication Conference*, (Optical Society of America, 2019), pp. W4E–3.
26. Z. Zhang, K. Zou, H. Wang, P. Liao, N. Satyan, G. Rakuljic, A. E. Willner, and A. Yariv, "High-speed coherent optical communication with isolator-free heterogeneous si/iii-v lasers," J. Light. Technol. **38**(23), 6584–6590 (2020).
27. M. A. Tran, D. Huang, and J. E. Bowers, "Tutorial on narrow linewidth tunable semiconductor lasers using si/iii-v heterogeneous integration," APL Photonics **4**(11), 111101 (2019).
28. M. A. Tran, D. Huang, J. Guo, T. Komljenovic, P. A. Morton, and J. E. Bowers, "Ring-resonator based widely-tunable narrow-linewidth si/inp integrated lasers," IEEE J. Sel. Top. Quantum Electron. **26**(2), 1–14 (2020).
29. S. McCall and P. Platzman, "An optimized $\pi/2$ distributed feedback laser," IEEE J. Quantum Electron. **21**(12), 1899–1904 (1985).
30. K. Petermann, *Laser diode modulation and noise*, vol. 3 (Springer Science & Business Media, 1991).